Nano Today 54 (2024) 102131

Contents lists available at ScienceDirect

Nano Today

journal homepage: www.elsevier.com/locate/nanotoday

Electrochemiluminescence of hot exciton nanomaterial with boosted efficiency for visual bioanalysis

Chao Wang [a], Lijuan Cui [b], Jie Wu [a], Xiangfu Hu [a], Xiaotian Wu [c], Zhonghua Cui [b], Huangxian Ju [a,*]

[a] State Key Laboratory of Analytical Chemistry for Life Science, School of Chemistry and Chemical Engineering, Nanjing University, Nanjing 210023, PR China
[b] Key Laboratoryof Physics and Technology for Advanced Batteries (Ministry of Education), Jilin University, Changchun 130023, PR China
[c] Research & Development Center, Canon Medical Systems (China) Co., LTD., Beijing 100015, PR China

ARTICLE INFO

Keywords:
Electrochemiluminescence
Organic nanomaterials
Hot exciton
Imaging
Electrochemiluminescence emitters
HPV

ABSTRACT

The electrochemiluminescence (ECL) efficiency (Φ_{ECL}) of organic ECL emitters is greatly influenced by the excited state property and component. Here we design a hot exciton molecule (BCzP-BT) with hybridized local and charge-transfer (HLCT) excited state property to prepare the first hot exciton organic nanorods (BB NRs). The BB NRs exhibit both sensitive annihilation and intense coreactant ECL emissions with a band gap emission model. Due to the reverse intersystem crossing among high-lying excited states (*h*RISC), the HLCT excited state property leads to highly efficient utilization of triplet excitons and thus high photoluminescence quantum yields (Φ_{PL}) of more than 80% at 554 nm, which is demonstrated by solvatochromic experiments and quantum chemical calculations. The high Φ_{PL} endows BB NRs with superior Φ_{ECL} over other nanoemitters, even the thermally activated delayed fluorescence materials, and thus offers highly-efficient nanoemitters for the design of ECL imaging strategy. As a proof of concept, an ECL probe is constructed by assembling BHQ2-ssDNA on BB NRs to integrate CRISPR/Cas12a system for target recognition, which produces a rapid and high-throughput ECL imaging platform. The proposed imaging method for HPV16 DNA detection shows excellent performance with a detection limit of 0.6 fM. This work broadens the application of hot exciton materials in ECL field, and opens a new avenue for developing next-generation ECL devices.

Introduction

Electrochemiluminescence (ECL), a light-emitting phenomenon occurs when the electrochemically generated excited state species transit radiatively to ground state, has become a potent analytical technique due to its negligible background and desirable spatiotemporal controllability [1,2]. Organic luminophores such as polyaromatic hydrocarbons [3], BODIPY derivatives [4], and fluorene-based polymers [5] are the earliest subjects of ECL studies in nonaqueous solvents. The emerging of reprecipitation method [6] popularizes the synthesis of organic nanomaterials, such as 9,10-diphenylanthracene nanoblocks [7], perylene nanocrystals [8] and conjugated polymer based dots (Pdots) [9,10], and their application in ECL bioanalysis. Despite the relatively high photoluminescence quantum yield (Φ_{PL}) of these organic nanomaterials, their ECL efficiency (Φ_{ECL}) is still unsatisfactory. The Φ_{ECL} is closely related to both the Φ_{PL} and the exciton utilization efficiency (η) [11], and the η of traditional organic luminophores is less than ~25% due to the spin statistical limitation (Scheme 1A, left) [12–14]. To harness the non-radiative (NR) triplet excitons, our recent work devised thermally activated delayed fluorescence (TADF) Pdots as ECL emitters to boost the exciton utilization efficiency and achieve an anodic Φ_{ECL} of 49.9% vs $Ru(bpy)_3^{2+}$ [15]. However, the Φ_{ECL} of TADF Pdots do not meet our expectation because the completely-separated frontier molecular orbitals induce charge transfer (CT) characters of both the lowest singlet (S_1) and triplet (T_1) excited states of TADF compounds, which causes low Φ_{PL} [16,17]. Meanwhile, the sluggish reverse intersystem crossing (RISC) of TADF compounds from T_1 to S_1 may result in severe annihilation due to the accumulation of long-lived triplet excitons in T_1 state (Scheme 1A, middle) [18].

As opposite to the RISC pathway of TADF compounds, the RISC of hot exciton materials occurs among the high-lying excited states (*h*RISC, $T_m \rightarrow S_n$, $m \geq 2$, $n \geq 1$), in which the large T_m-T_1 energy gap inhibits the internal conversion (IC) from T_m to T_1, and the narrow T_m-S_n energy splitting promotes the *h*RISC (Scheme 1A, right) [19,20]. Accordingly,

* Corresponding author.
E-mail address: hxju@nju.edu.cn (H. Ju).

https://doi.org/10.1016/j.nantod.2023.102131
Received 28 May 2023; Received in revised form 12 October 2023; Accepted 18 December 2023
Available online 23 December 2023

hot exciton materials can more sufficiently utilize triplet excitons than TADF materials for energy radiation because the accelerated *h*RISC process alleviates the quenching of T_1 excitons [21,22]. Moreover, different from the strong CT character of TADF materials, the hybridized local and charge-transfer (HLCT) excited state property of hot exciton materials, in which the S_1 state is a locally excited (LE) or LE-dominated HLCT state and the T_m and S_n states are CT states, endows them with both high Φ_{PL} and the η up to 100% [23], which promotes their application in organic light-emitting diode [24–26].

Inspired by the high η of CT state and the high Φ_{PL} of LE state [27], this work designed a novel ECL nanoemitter with a hot exciton molecule for attaining high Φ_{ECL}. Using 4,7-dibromobenzo[*c*][1,2,5]thiadiazole (BT) with high luminous efficiency as the electron acceptor and 9-[4-(4,4,5,5-tetramethyl-1,3,2-dioxaborolan-2-yl)phenyl]carbazole (CzP) with rigid plane structure as the electron donor, a kind of hot exciton molecule, 4,7-bis(4-(9 H-carbazol-9-yl)phenyl)benzo[*c*][1,2,5]thiadiazole (BCzP-BT) with HLCT excited state, was synthesized via a Suzuki coupling reaction (Scheme 1B). The corrsponding nanomaterial, BCzP-BT nanorods (BB NRs), was thus prepared via simple reprecipitation. Both BCzP-BT in tetrahydrofuran (THF) and BB NRs in water showed fluorescence (FL) emissions with Φ_{PL} of 84.0% and 89.3% at 554 nm respectively, and their HLCT excited state property were identified by solvatochromic experiments and quantum chemical calculations. The BB NRs exhibited sensitive annihilation ECL and intense coreactant ECL emissions with high Φ_{ECL}, offering a highly efficient ECL emitter for designing ECL imaging strategy. By using Au/ITO as the substrate to load black hole quencher 2 (BHQ2)-ssDNA modified BB NRs and CRISPR/Cas12a system for target recognition, a rapid and high-throughput ECL imaging platform was constructed for detection of human papilloma virus subtype HPV16 DNA, which demonstrated a wide detection range and desirable sensitivity, indicating the promising application of hot exciton based organic nanomaterials as highly efficient ECL nanoemitters.

Results and discussion

Hot exciton property of BCzP-BT

The synthesis of BCzP-BT was verified by ^{1}H NMR and MALDI-TOF-MS spectroscopy (Fig. S1 and S2). The molecular configuration of BCzP-BT showed a large torsional angle between carbazole (Cz) and its adjacent benzene ring (Scheme 1C) due to the steric effect of hydrogen atoms, which could suppress the nonradiative decay and avoid intermolecular accumulation induced quenching. The photophysical properties of BCzP-BT in different solvents (Table S1) could be obtained from its normalized UV–vis absorption and FL spectra (Fig. 1A). Due to the intramolecular charge transfer from Cz to BT unit, BCzP-BT exhibited a broad absorption around 400 nm with negligibly-changed shape and position in different solvents. Contrarily, with the increasing of solvent polarity, the FL spectra of BCzP-BT displayed a 68 nm bathochromic-shift and the FL peak broadened, indicating a strong CT character. Moreover, the difference between the FL spectra of CzP, BT and BCzP-BT (Fig. S3) indicated that the luminescence originated from the charge transfer from Cz to BT rather than the subunit itself.

To probe the excited state property of BCzP-BT, the relationship between Stokes shift (ν_a-ν_f) and the orientation polarizability (Δf) of solvent was examined for estimating the dipole moment of S_1 according to Lippert-Mataga solvatochromic model [28,29]. The plot showed

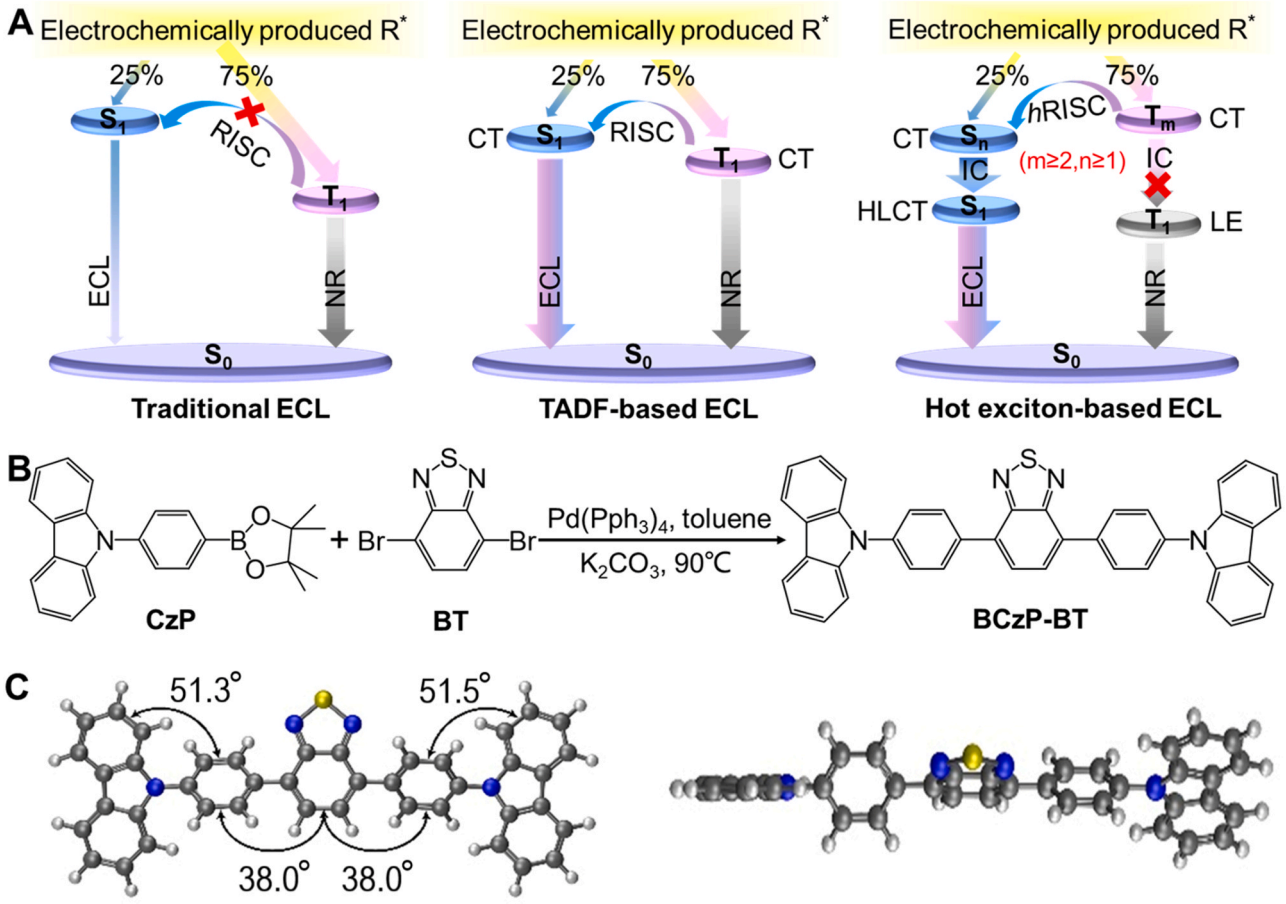

Scheme 1. Schematic diagrams of (A) traditional, TADF-based and hot exciton-based ECL systems, (B) synthetic route of BCzP-BT, and (C) side and top views of BCzP-BT at B3LYP/6–31 G(d, p) level.

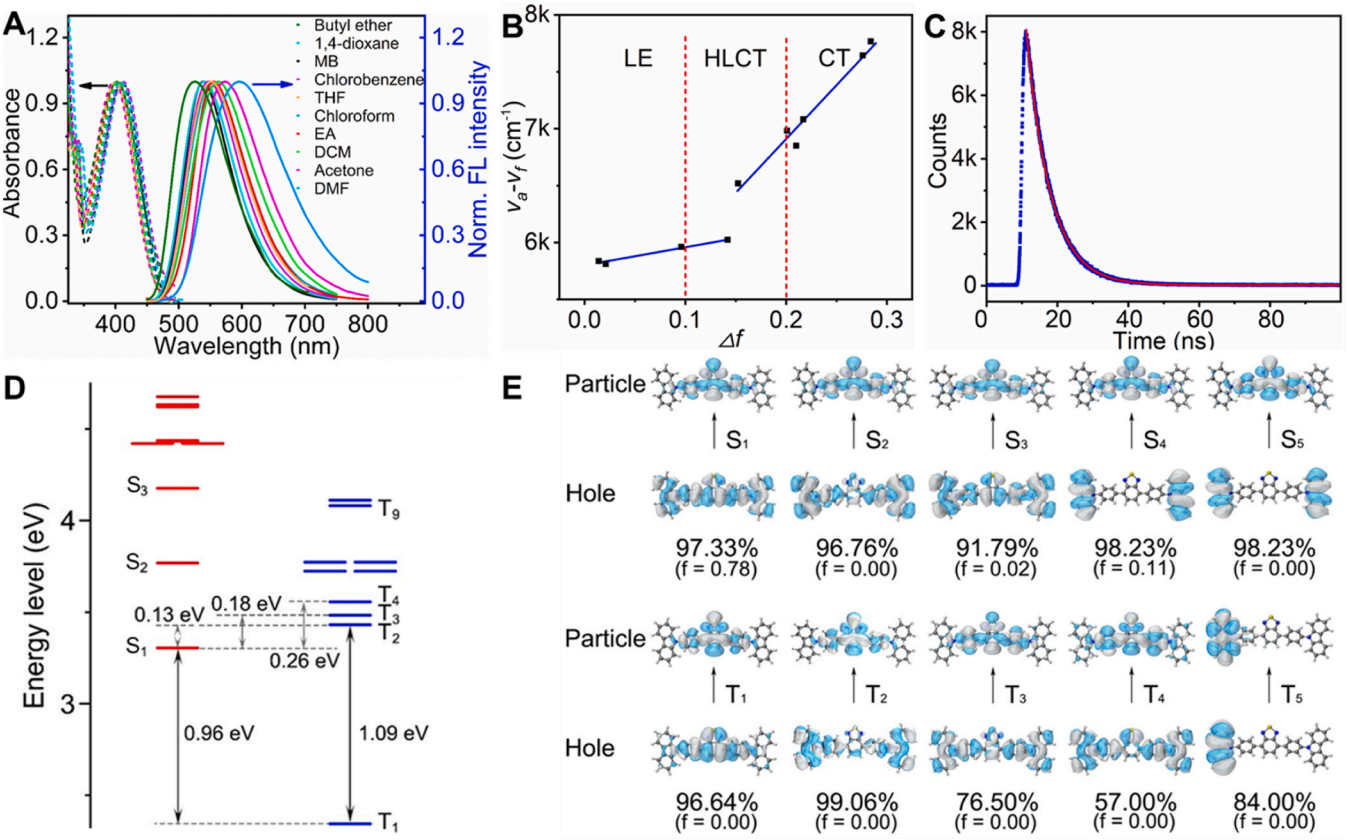

Fig. 1. Verification the hot exciton property of BCzP-BT. (A) Normalized UV–vis absorption and FL spectra of BCzP-BT in different solvents. (B) Plot of Stokes shift (ν_a-ν_f) for BCzP-BT vs orientation polarization (Δf) of solvent. (C) Transient PL decay curve of BCzP-BT in THF. (D) Excited state energy diagram of BCzP-BT, including the lowest ten singlet and ten triplet excited states at TD-M062x/6–31 G(d, p) level. (E) Natural transition orbitals of BCzP-BT in the first 5 singlet and triplet excited states (*f* is the oscillator strength, and the percentage represents the transition possibility).

two-section fitted lines with a small dipole moment for BCzP-BT in low-polarity solvents and a large dipole moment for BCzP-BT in high-polarity solvents (Fig. 1B), which corresponded to the S_1 excited states of LE- and CT-dominates of BCzP-BT, respectively. As for BCzP-BT in medium-polarity solvents, the excited state exhibited the properties of both LE- and CT-states. The fluorescence lifetime of BCzP-BT showed a mono-exponential decay of 6.72 ns without delay (Fig. 1C), further proving that the S_1 excited state of BCzP-BT was a HLCT excited state rather than a simple mixing of LE and CT state.

To verify the possibility of hot exciton process, the lowest ten singlet and ten triplet excited states of BCzP-BT were evaluated. The large energy gap between T_2 and T_1 (1.09 eV) suppressed the IC from T_2 to T_1, while the narrow energy gap between T_2 and S_1 (0.13 eV) facilitated the *h*RISC from T_2 to S_1 (Fig. 1D, Table S2), thus alleviating the triplet exciton accumulation induced quenching and enabling the effective utilization of triplet excitons via hot exciton channel. The natural transition orbitals (NTOs) of BCzP-BT (Fig. 1E) showed the LE state of T_1 and the CT states of S_m and T_n, and the intercrossed LE and CT state of S_1 as the particles of S_1 were localized on BT and its adjacent benzene ring, whereas the holes were distributed on the whole skeleton.

Characterization of BB NRs

The BB NRs prepared by reprecipitation of BCzP-BT with poly (styrene-co-maleic anhydride) (PSMA) as a carboxyl-functionalized copolymer displayed slender rod morphologies with an average diameter of 27 nm and length of 180 nm (Fig. 2A and B). The BB NRs dispersion was light green under daylight whereas emitted bright yellowish green light under 365 nm UV irradiation (Fig. 2C). Compared with BCzP-BT, BB NRs showed a slight redshift in UV–vis absorption around 400 nm (Fig. 2D) due to the polarization environment of BB NRs in water, which reduced the transition energy [30]. Both BCzP-BT and BB NRs showed similar FL emission peaks at 554 nm and prompt FL lifetimes of about 6.7 ns (Fig. 2D and E), revealing that BB NRs inherited the photophysical properties from BCzP-BT. The Φ_{PL} of BCzP-BT in air-saturated THF and BB NRs in water were 84.0% and 89.3% respectively, higher than 73.7% of the previously reported TADF Pdots [15], which could be attributed to the existence of HLCT state in the S_1 excited state of BB NRs, whereas only the existence of CT state in the S_1 excited state of TADF Pdots.

Annihilation and coreactant ECL behaviors of BB NRs

Annihilation ECL experiments were conducted to examine the stability of radical intermediates of BB NRs. In N_2-saturated PBS, the cyclic voltammogram (CV) of BB NRs modified glassy carbon electrode (GCE) showed an oxidation peak at + 0.95 V due to the oxidation of Cz and a reduction peak at − 1.45 V due to the reduction of BT, which resulted in a weak ECL emission at + 1.05 V when the potential was scanned anodically first (Fig. 3A, curve a) and relatively strong ECL emissions at both + 1.05 V and − 2.0 V when the potential was scanned cathodically first (Fig. 3A, curve b), revealing the more stable reduced states of BB NRs. Moreover, the transient ECL emission of BB NRs occurred at + 1.50 V only after the potential was stepped from − 2.0 V to + 1.5 V (Fig. 3B), confirming the better stability of BB NRs$^{\cdot-}$ [31].

An irreversible oxidation peak of tripropylamine (TPrA) at bare GCE could be observed at + 0.98 V with an onset potential of + 0.57 V (Fig. 4A, curve a), in which TPrA$^{\cdot}$ radical was generated after the oxidation product TPrA$^{\cdot+}$ deprotonated. The CV of BB NRs/GCE showed the oxidation of BB NRs started near + 0.70 V to produce cationic

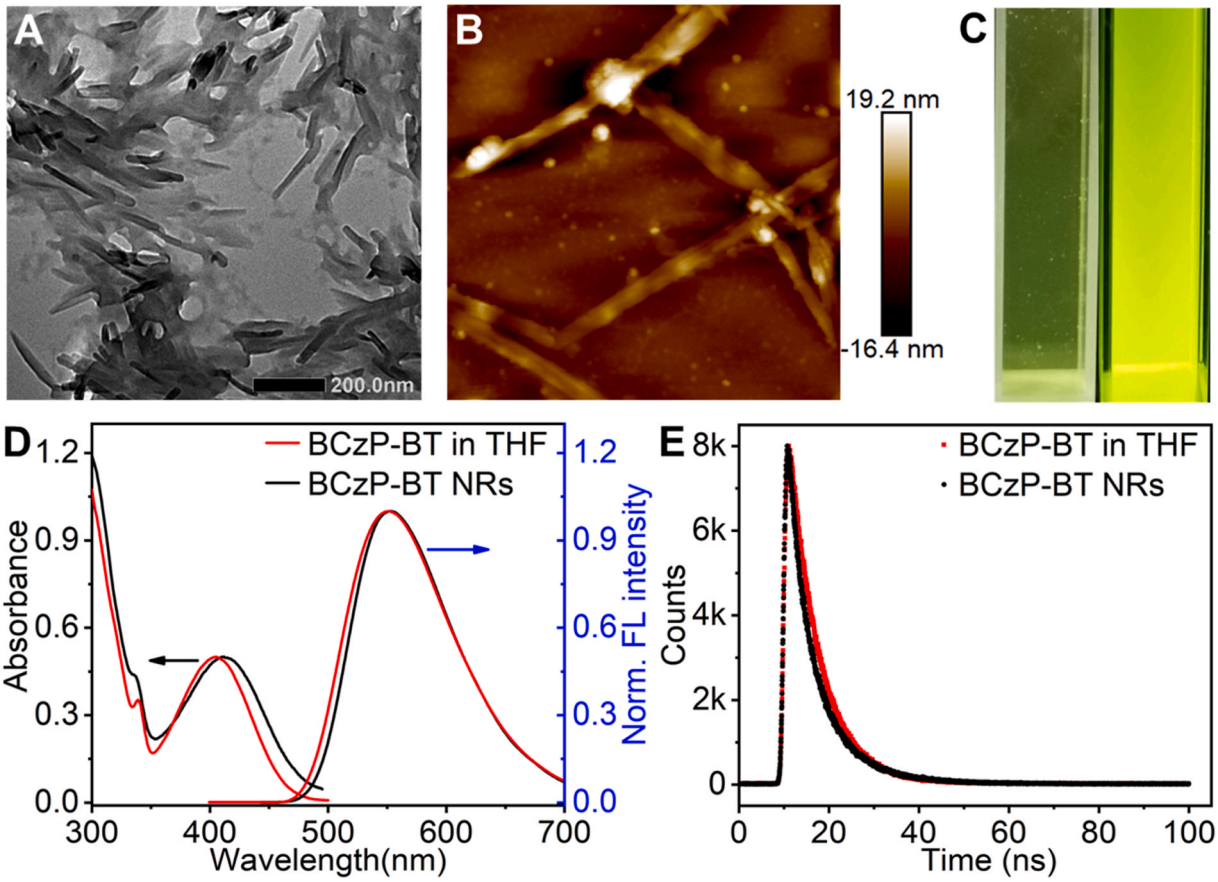

Fig. 2. Characterization of BB NRs. (A) TEM and (B) AFM images of BB NRs. (C) Photographs of BB NRs dispersion under daylight (left) and 365 nm irradiation (right). (D) UV–vis absorption and FL spectra, and (E) transient PL decay curves of BCzP-BT and BB NRs.

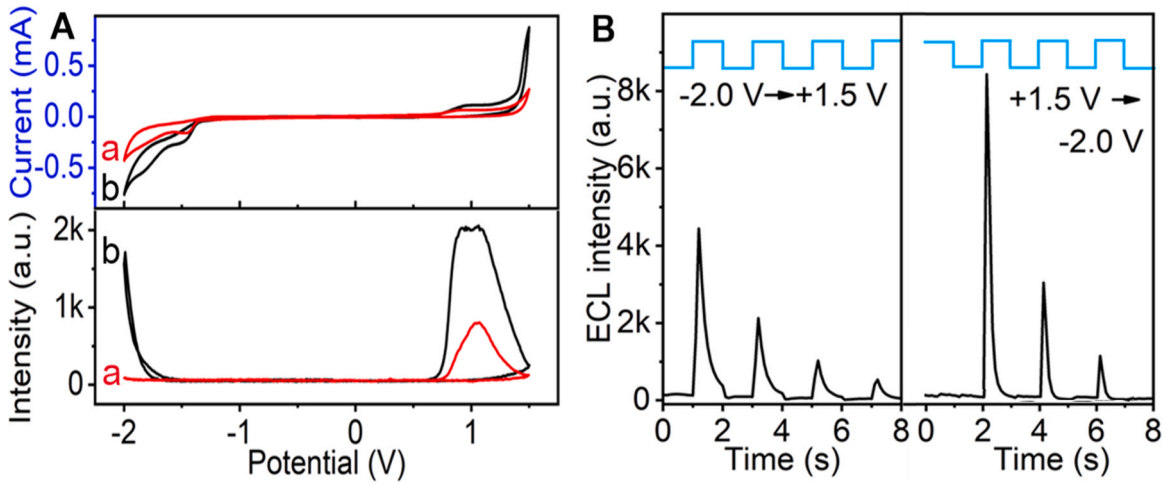

Fig. 3. Annihilation ECL behavior of BB NRs. (A) CV (top) and ECL (bottom) curves of BB NRs/GCE in N_2-saturated 0.1 M pH 7.4 PBS (a) from 0 to + 1.5 and then − 2.0 V, and (b) from 0 to − 2.0 V and then + 1.5 V. (B) ECL transients of BB NRs/GCE in N_2-saturated 0.1 M pH 7.4 PBS with steps from − 2.0 to + 1.5 V (left) and + 1.5 to − 2.0 V (right). PMT: 800 V.

radical BB NRs$^{\cdot+}$, which caused very weak ECL emission (Fig. 4A and B, curve b). In the presence of TPrA, both the oxidation peaks of TPrA and BB NRs were observed at BB NRs/GCE, and an intensive ECL emission peak occurred at + 1.07 V (Fig. 4A and B, curve c), which was ascribed to the radiative relaxation of excited BB NRs (BB NRs*) produced by the charge transfer between TPrA$^{\cdot}$ and BB NRs$^{\cdot+}$, along with the rapid transfer of triplet excitons to singlet state via hot exciton channel (Fig. 4C) [15]. In cathodic process, $S_2O_8^{2-}$ could be reduced at GCE with a peak around − 1.07 V to produce the strong oxidizing $SO_4^{\cdot-}$ and very weak ECL emission (Fig. 4D and E, curve a), while BB NRs/GCE showed an obvious reduction peak at − 1.55 V to produce BB NRs$^{\cdot-}$ (Fig. 4D, curve b). In the presence of $K_2S_2O_8$, BB NRs/GCE showed the overlapped reduction peaks of BB NRs and $S_2O_8^{2-}$ around − 1.40 V, and an intensive ECL emission (Fig. 4D and E, curve c), which was due to the radiative decay of BB NRs* generated from the reaction between BB NRs$^{\cdot-}$ and $SO_4^{\cdot-}$ (Fig. 4F).

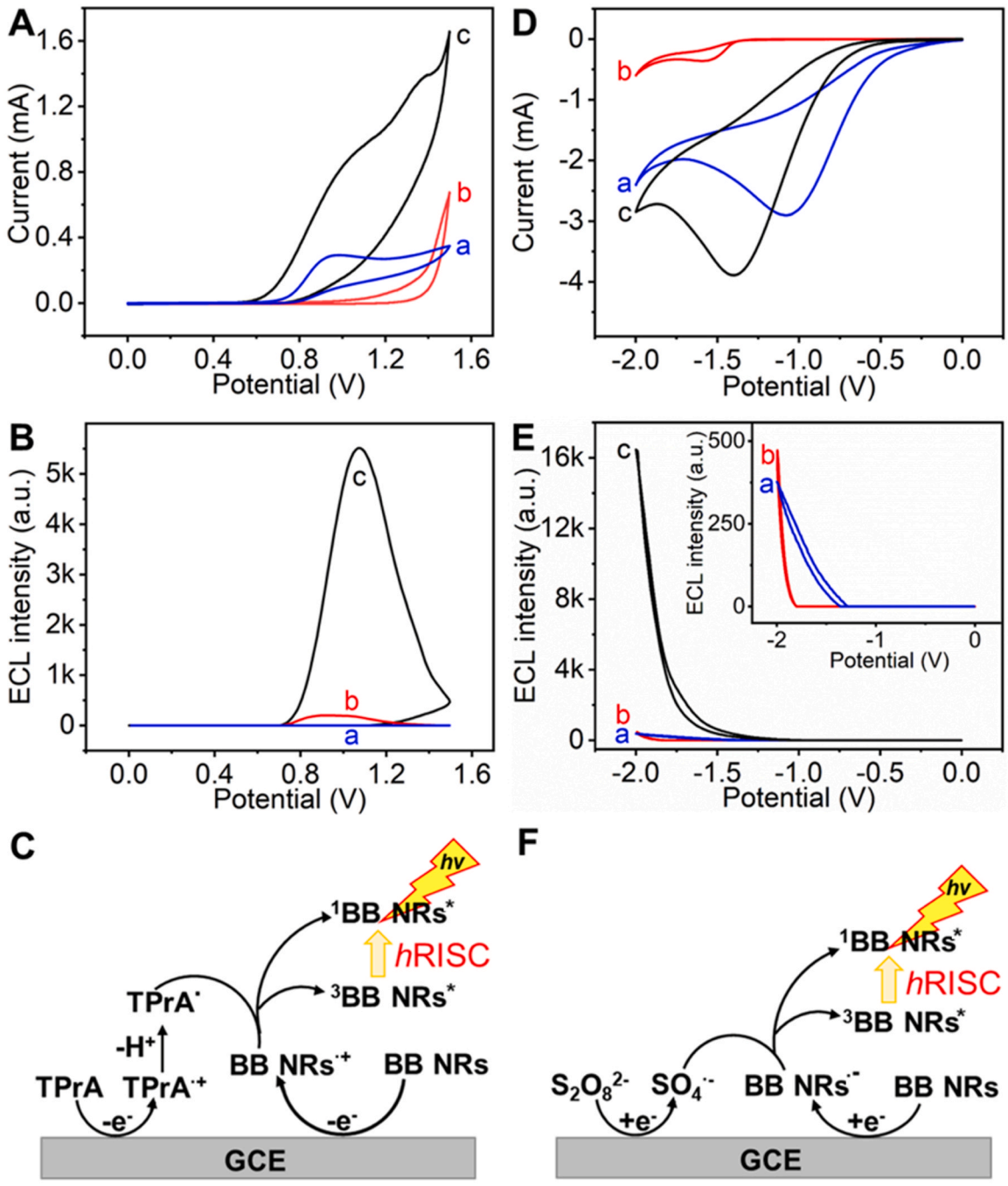

Fig. 4. Coreactant ECL behavior of BB NRs. (A) CV and (B) ECL curves of bare (a) and BB NRs modified (b,c) GCE in 0.1 M pH 7.4 PBS in absence (b) and presence (a, c) of 10 mM TPrA. (C) Anodic ECL mechanism of BB NRs in presence of TPrA. (D) CV and (E) ECL curves of bare (a) and BB NRs modified (b,c) GCE in 0.1 M pH 7.4 PBS in absence (b) and presence (a,c) of 0.1 M $K_2S_2O_8$. (F) Cathodic ECL mechanism of BB NRs in presence of $K_2S_2O_8$. PMT: 400 V (B) and 600 V (D).

As the precursor of BB NRs, BCzP-BT showed an oxidation peak at + 1.38 V in tetrahydrofuran containing 0.1 M tetra-n-butyl-ammonium perchlorate (Fig. S4A), which resulted in the ECL emission peaked at + 1.08 V in the presence of 10 mM TPrA (Fig. S4B), which showed another oxidation peak at + 1.15 V, demonstrating the potential of BCzP-BT as a novel ECL emitter. Compared with BB NRs/GCE (Fig. 4B, E), the BCzP-BT/GCE displayed much weaker anodic and cathodic ECL emissions (Fig. S4C-F), demonstrating that the reprecipitation method is an effective strategy to improve the hydrophilicity of synthesized BB NRs and alleviate the quenching effect of oxygen towards triplet excitons, and thus enhancing the ECL intensity of hot exciton materials.

ECL route and efficiency of BB NRs

The anodic and cathodic ECL emission peaks of BB NRs at 560 nm were well matched with the FL emission peak (Fig. S5A), inferring that the ECL and FL processes of BB NRs shared the same excited state produced via band gap transition [32]. The CV of BB NRs in N_2-saturated THF (Fig. S5B) displayed an oxidation peak and two consecutive reduction peaks in positive potential range due to the presence of two terminal Cz groups, while the two electron-withdrawing imine bonds (C═N) in BT group led to two reduction peaks in negative potential range [33,34]. The simulated highest occupied molecular orbital (HOMO) was distributed on the entire conjugated skeleton, whereas the

lowest unoccupied molecular orbital (LUMO) was centered on the BT and its neighboring phenyls (Fig. S5C), and the simulated energy gap (E_g) of 2.70 eV was a little bigger than that of 2.28 eV calculated from CV data and the optical gap (E_s) of 2.24 eV (Table S3), suggesting the semiconductor feacture of BB NRs. Meanwhile, larger annihilation enthalpy (-Δ*H*) of 2.55 eV than E_s (Table S3) resulted in sufficient energy release to generate both singlet and triplet excitons, and the excitons at high-lying triplet states could then transfer to S_1 state via hot exciton pathway to achieve the radiative decay from S_1 to S_0. Thus the exciton utilization efficiency could theoretically be up to 100%, which greatly boosted the ECL efficiency [15]. By using 1 mM $Ru(bpy)_3^{2+}$ as the standard, the anodic and cathodic ECL efficiencies of BB NRs in the presence of 10 mM TPrA or 100 mM $K_2S_2O_8$ (Fig. S6) were calculated to be 56.7% and 24.6%, respectively (Table S4) [35], which were higher than those of traditional fluorescence-based Pdots [9,10,32,36,37] and TADF Pdots [15] (Table S5). The high anodic ECL efficiency meant that the BB NRs could be used as an excellent emitter for ECL imaging analysis.

Construction and characterization of ECL imaging array

To attest the application of BB NRs in ECL imaging, BHQ2-labeled ssDNA was covalently linked onto BB NRs to prepare the ECL probe (Fig. 5A), which was then coated on Au/ITO to form a "signal off" ECL imaging chip (Fig. 5B). Using HPV16 DNA as a target model (Table S6), the "signal on" ECL imaging chip could be obtained for target-related signal collection after HPV16 DNA activated CRISPR/Cas12a was dropped on the chip to release BHQ2 from BB NRs. The presence of deposited Au layer could greatly improve both the electrochemical and ECL behaviors of BB NRs on ITO (Fig. S7) [38]. The successful preparation of BB NRs-DNA was confirmed by UV–vis absorption spectra, which showed both the absorption peaks of BB NRs and the characteristic absorption of DNA-BHQ2 at 260 nm and 580 nm (Fig. S8A). After linking DNA onto BB NRs, the Zeta potential became more negative (Fig. S8B). The broad absorption band of BHQ2 overlapped well with the FL emission peak of BB NRs (Fig. S8A), demonstrating that BHQ2 could quench the emission of BB NRs via resonance energy transfer.

Electrophoretic analysis was conducted to prove the cleavage ability of activated CRISPR/Cas12a. Upon the recognition of Cas12a enzyme to the T nucleotide-rich protospacer- adjacent motif (PAM) of target HPV16 DNA in the presence of crRNA [39], the band of target DNA disappered, and the ssDNA cleavage activity of CRISPR/Cas12a was triggered to digest ssDNA, which resulted in the disappearance of ssDNA band (Fig. S9). The recovery of both FL and ECL emission after adding target-activated CRISPR/Cas12a to BB NRs-DNA further proved the ssDNA cleavage ability (Fig. S10). From the ECL intensity profiles

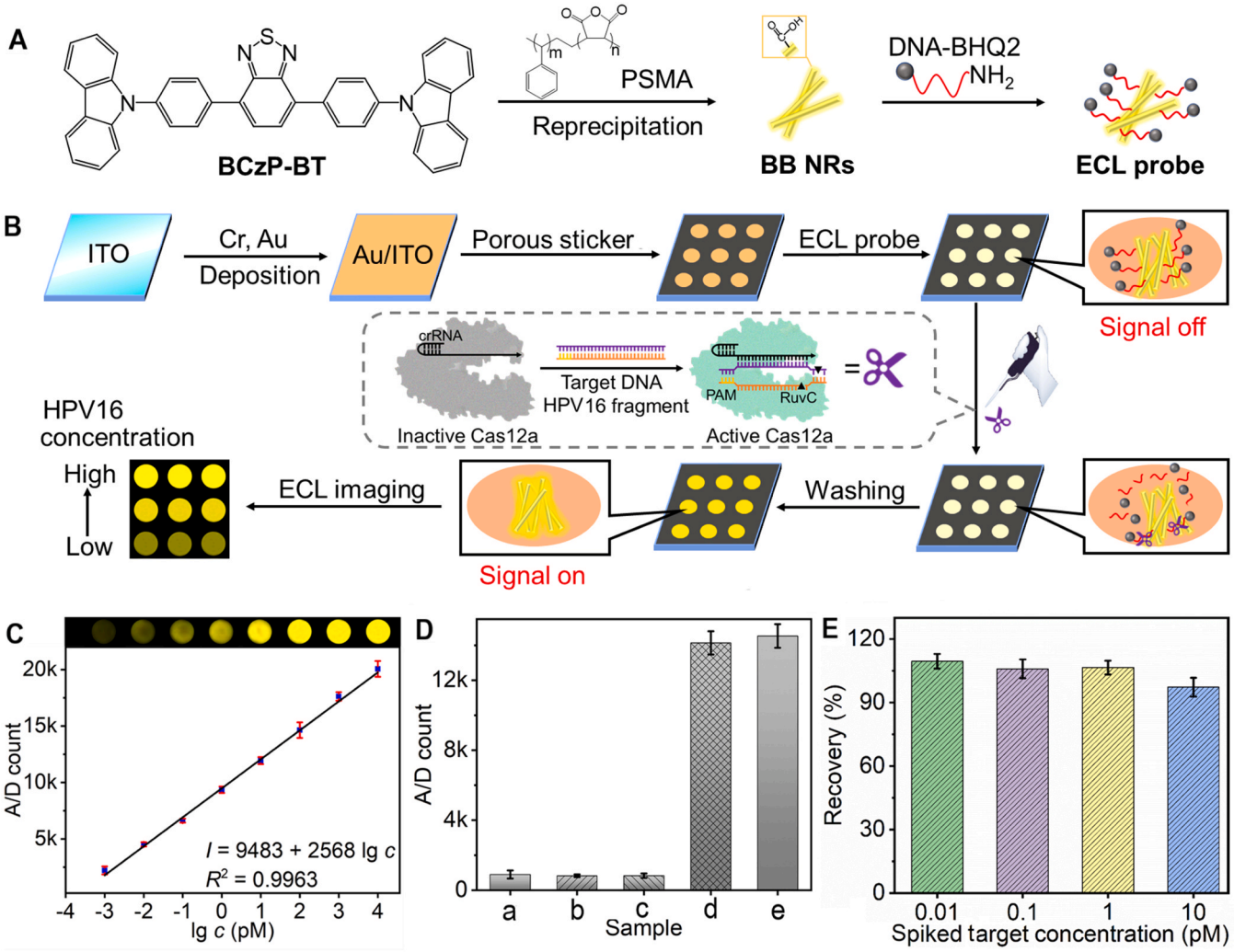

Fig. 5. Fabrication of ECL imaging array and its analytical performance for HPV16 DNA detection. Schematic diagrams of (A) preparation of ECL probe, and (B) fabrication of ECL imaging array for detection of HPV16 DNA. (C) ECL images at different HPV16 DNA concentrations and calibration curve for HPV16 DNA detection. (D) Responses of the proposed imaging method to 1 nM HPV18 (a), HPV31 (b) and HPV58 (c), 100 pM HPV16 (d), and the mixture of (a-d) (e). (E) Recovery of different concentrations of HPV16 spiked in 10 × diluted human serum sample ($n = 3$).

(Fig. S10B), the quenching efficiency of DNA-BHQ2 to BB NRs was calculated to be 95.6%, while the activated CRISPR/Cas12a system achieved the recovery of 76.0%. The high quenching efficiency, low background (Fig. S10B, curve d), and strong recovery ability endowed the ECL imaging platform with excellent visual performance.

Performance of ECL imaging detection of HPV16 DNA

To realize the sensitive ECL imaging detection of HPV16 DNA, the concentrations of Cas12a and crRNA and the cleavage time of DNA-BHQ2 by the target-activated CRISPR/Cas12a were optimized to be 50 nM, 75 nM and 40 min, respectively (Fig. S11). Under the optimal conditions, the ECL images became brighter as the concentration of HPV16 DNA increased from 1 fM to 10 nM (Fig. 5C), which showed a linear plot of ECL intensity integration vs the logarithm of HPV16 DNA concentration with a limit of detection of 0.6 fM at a signal-to-noise ratio of 3. Compared with other electrochemical biosensing methods for HPV16 DNA (Table S7), the proposed ECL imaging strategy displayed the widest detection range and the lowest limit of detection except one amperometric biosensing method [40]. Although this previously reported method showed a lower limit of detection, it needed an additional signal amplification procedure including entropy-driven target recycling and hyperbranched rolling circle amplification, which was operated with 8 steps and about 6 h [40]. Obviously, the proposed method greatly simplified the operation procedure, shortened the analytical time, and also lowered the detection cost.

The specificity of the proposed ECL imaging method was verified with 1 nM HPV18, HPV31, and HPV58 DNA as the interferents, which showed negligible response compared with 0.1 nM HPV16 DNA (Fig. 5D). The mixture of these interferents with HPV16 DNA also showed the same signal as that of the target alone, implying the excellent specificity. The application potential of this strategy was further examined by spiking various concentrations of HPV16 DNA into human serum samples. The recoveries were in the range of 97%– 109% (Fig. 5E). Therefore, this work provided both a highly efficient ECL nanoemitter and a rapid and high-throughput detection technique for HPV16 DNA analysis in complex biosamples.

Conclusion

This work has designed a hot exciton molecule BCzP-BT with benzothiadiazole as the acceptor and carbazole as the donor for developing highly efficient ECL nanoemitters. This molecule possesses HLCT excited state property, suppressed IC from T_2 to T_1, and facilitated *h*RISC from T_2 to S_1, leading to a Φ_{PL} of 84.0%. Using BCzP-BT as a precursor, BB NRs with high exciton utilization efficiency and a Φ_{PL} of 89.3% have been synthesized, which show sensitive annihilation ECL and intense coreactant ECL emissions with superior Φ_{ECL} over other nanoemitters. Benifitting from the high anodic Φ_{ECL}, a rapid and high-throughput ECL imaging chip has also been constructed by coating BHQ2-ssDNA linked BB NRs on Au/ITO and combining a target-activated CRISPR/Cas12a system. The proposed ECL imaging method for HPV16 DNA shows excellent performance with wide detection range, low limit of detection, simple operation and high specificity, and can be extended for other DNA detections by changing the target-related crRNA, demonstrating promising application of the hot exciton materials in ECL field.

CRediT authorship contribution statement

C.W.: Conceptualization, Data Curation, Formal analysis, Writing - original draft. **L.C.**: Conceptualization, Formal analysis. **J.W.:** Project administration, Funding acquisition. **X.H.:** Methodology, Resources. **X.W.:** Validation, Resources. **Z.C.:** Formal analysis, Software. **H.J.:** Funding acquisition, Supervision, Writing - original draft.

Declaration of Competing Interest

The authors declare that they have no known competing financial interests or personal relationships that could have appeared to influence the work reported in this paper.

Data availability

No data was used for the research described in the article.

Acknowledgments

We gratefully acknowledge the financial supports from the National Natural Science Foundation of China (21890741), the Canon Medical Systems Corp. (2022200494), and the Science and Technology Project of Nanjing City (202110023).

Appendix A. Supporting information

Supplementary data associated with this article can be found in the online version at doi:10.1016/j.nantod.2023.102131.

References

[1] Z.Y. Liu, W.J. Qi, G.B. Xu, Chem. Soc. Rev. 44 (2015) 3117–3142.
[2] L. Wang, Z.G. Wang, D. Ning, Y. Hu, S.L. Liu, D.W. Pang, Nano Today 50 (2023), 101855.
[3] K.M. Omer, S.-Y. Ku, K.-T. Wong, A.J. Bard, Angew. Chem. Int. Ed. 48 (2009) 9300–9303.
[4] A.B. Nepomnyashchii, S. Cho, P.J. Rossky, A.J. Bard, J. Am. Chem. Soc. 132 (2010) 17550–17559.
[5] H.L. Qi, J. Chang, S.H. Abdelwahed, K. Thakur, R. Rathore, A.J. Bard, J. Am. Chem. Soc. 134 (2012) 16265–16274.
[6] K.M. Omer, S. Ku, J. Cheng, S. Chou, K. Wong, A.J. Bard, J. Am. Chem. Soc. 133 (2011) 5492–5499.
[7] J.L. Liu, Z.L. Tang, J.Q. Zhang, Y.Q. Chai, Y. Zhuo, R. Yuan, Anal. Chem. 90 (2018) 5298–5305.
[8] J. Zhao, J. Da, S.S. Yang, Y.M. Lei, Y.Q. Chai, R. Yuan, Y. Zhuo, Electrochim. Acta 332 (2020), 135389.
[9] Z.Y. Wang, J.B. Pan, Q. Li, Y. Zhou, S. Yang, J.J. Xu, D.B. Hua, Adv. Funct. Mater. 30 (2020), 2000220.
[10] N.N. Wang, Z.Y. Wang, L.Z. Chen, W.W. Chen, Y.W. Quan, Y.X. Cheng, H.X. Ju, Chem. Sci. 10 (2019) 6815–6820.
[11] A.J. Bard, Electrogenerated Chemiluminescence, Marcel Dekker, New York, 2004.
[12] R. Ishimatsu, S. Matsunami, T. Kasahara, J. Mizuno, T. Edura, C. Adachi, K. Nakano, T. Imato, Angew. Chem. Int. Ed. 53 (2014) 6993–6996.
[13] B.H. Zhang, Y. Kong, H.J. Liu, B. Chen, B.L. Zhao, Y.L. Luo, L.J. Chen, Y.W. Zhang, D.X. Han, Z.J. Zhao, B.Z. Tang, L. Niu, Chem. Sci. 12 (2021) 13283–13291.
[14] S.Q. Yu, Y. Du, X.H. Niu, G.M. Li, D. Zhu, Q. Yu, G.Z. Zou, H.X. Ju, Nat. Commun. 13 (2022) 7302.
[15] C. Wang, J. Wu, H. Huang, Q.Q. Xu, H.X. Ju, Anal. Chem. 94 (2022) 15695–15702.
[16] X.Y. Tang, Q. Bai, Q.M. Peng, Y. Gao, J.Y. Li, Y.L. Liu, L. Yao, P. Lu, B. Yang, Y. G. Ma, Chem. Mater. 27 (2015) 7050–7057.
[17] W.J. Li, Y. Pan, R. Xiao, Q.M. Peng, S.T. Zhang, D.G. Ma, F. Li, F.Z. Shen, Y. H. Wang, B. Yang, Y.G. Ma, Adv. Funct. Mater. 24 (2014) 1609–1614.
[18] S.T. Zhang, L. Yao, Q.M. Peng, W.J. Li, Y.Y. Pan, R. Xiao, Y. Gao, C. Gu, Z.M. Wang, P. Lu, F. Li, S.J. Su, B. Yang, Y.G. Ma, Adv. Funct. Mater. 25 (2015) 1755–1762.
[19] Y.W. Xu, P. Xu, D.H. Hu, Y.G. Ma, Chem. Soc. Rev. 50 (2021) 1030–1069.
[20] C. Wang, X.L. Li, Y.Y. Pan, S.T. Zhang, L. Yao, Q. Bai, W.J. Li, P. Lu, B. Yang, S. J. Su, Y.G. Ma, ACS Appl. Mater. Interfaces 8 (2016) 3041–3049.
[21] H. Zhang, J.N. Xue, C.L. Li, S.T. Zhang, B. Yang, Y. Liu, Y. Wang, Adv. Funct. Mater. 31 (2021), 2100704.
[22] C.W. Lin, P.B. Han, S. Xiao, F.L. Qu, J.W. Yao, X.F. Qiao, D.Z. Yang, Y.F. Dai, Q. Sun, D.H. Hu, A.J. Qin, Y.G. Ma, B.Z. Tang, D.G. Ma, Adv. Funct. Mater. 31 (2021), 2106912.
[23] T.T. Liu, X.J. Chen, J. Zhao, W.C. Wei, Z. Mao, W. Wu, S.B. Jiao, Y. Liu, Z.Y. Yang, Z.G. Chi, Chem. Sci. 12 (2021) 5171–5176.
[24] X.H. Lv, M.Z. Sun, L. Xu, R.Z. Wang, H.Y. Zhou, Y.Y. Pan, S.T. Zhang, Q.K. Sun, S. F. Xue, W.J. Yang, Chem. Sci. 11 (2020) 5058–5065.
[25] L.F. Chen, S.T. Zhang, H. Li, R.F. Chen, L. Jin, K. Yuan, H.H. Li, P. Lu, B. Yang, W. Huang, J. Phys. Chem. Lett. 9 (2018) 5240–5245.
[26] Y.L. Liu, H. Liu, Q. Bai, C.Y. Du, A.Q. Shang, D.Y. Jiang, X.Y. Tang, P. Lu, ACS Appl. Mater. Interfaces 12 (2020) 16715–16725.
[27] W.J. Li, Y.Y. Pan, L. Yao, H.C. Liu, S.T. Zhang, C. Wang, F.Z. Shen, P. Lu, B. Yang, Y.G. Ma, Adv. Opt. Mater. 2 (2014) 892–901.
[28] W.J. Li, D.D. Liu, F.Z. Shen, D.G. Ma, Z.M. Wang, T. Feng, Y.X. Xu, B. Yang, Y. G. Ma, Adv. Funct. Mater. 22 (2012) 2797–2803.

[29] J.J. Tong, Y. Cao, Y.W. Zhang, P. Wang, P.L. Wang, X.J. Liao, W.G. Zhang, Y. Wang, Y.X. Zheng, J.J. Zhu, Y. Pan, Angew. Chem. Int. Ed. 61 (2022), e202209438.
[30] K.M. Omer, A.J. Bard, J. Phys. Chem. C 113 (2009) 11575–11578.
[31] Z.C. Jin, X.R. Zhu, N.N. Wang, Y.F. Li, H.X. Ju, J.P. Lei, Angew. Chem. Int. Ed. 59 (2020) 10446–10450.
[32] Y.Q. Feng, C.H. Dai, J.P. Lei, H.X. Ju, Y.X. Cheng, Anal. Chem. 88 (2016) 845–850.
[33] K.M. Omer, S.-Y. Ku, Y.-C. Chen, K.-T. Wong, A.J. Bard, J. Am. Chem. Soc. 132 (2010) 10944–10952.
[34] K.M. Omer, S.-Y. Ku, K.-T. Wong, A.J. Bard, J. Am. Chem. Soc. 131 (2009) 10733–10741.
[35] M. Hesari, M.S. Workentin, Z.F. Ding, ACS Nano 8 (2014) 8543–8553.
[36] Z.Y. Wang, Y.Q. Feng, N.N. Wang, Y.X. Cheng, Y.W. Quan, H.X. Ju, J. Phys. Chem. Lett. 9 (2018) 5296–5302.
[37] Y.Q. Feng, N.N. Wang, H.X. Ju, Anal. Chem. 90 (2018) 1202–1208.
[38] S.L. Pan, J. Liu, C.M. Hill, J. Phys. Chem. C 119 (2015) 27095–27103.
[39] J.S. Chen, E. Ma, L.B. Harrington, M.D. Costa, X.R. Tian, J.M. Palefsky, J. A. Doudna, Science 360 (2018) 436–439.
[40] Y.H. He, L.J. Cheng, Y.Y. Yang, P. Chen, B. Qiu, L.H. Guo, Y. Wang, Z.Y. Lin, G. L. Hong, Sens. Actuators B-Chem. 320 (2020), 128407.